POLITECNICO DI TORINO
Repository ISTITUZIONALE

Experimental modelling uncertainty quantification for a prototype wave energy converter

Original
Experimental modelling uncertainty quantification for a prototype wave energy converter / Celesti, M.L., Ferri, F., Faedo, N.E.. - (2024), pp. 1546-1551. (European Control Conference (ECC) Stockholm (SWE) 25-28 June 2024) [10.23919/ECC64448.2024.10590984].

Availability:
This version is available at: 11583/2991026 since: 2024-08-06T15:07:27Z

Publisher:
European Control Conference (ECC)

Published
DOI:10.23919/ECC64448.2024.10590984

Terms of use:

This article is made available under terms and conditions as specified in the corresponding bibliographic description in the repository

Publisher copyright
IEEE postprint/Author's Accepted Manuscript

©2024 IEEE. Personal use of this material is permitted. Permission from IEEE must be obtained for all other uses, in any current or future media, including reprinting/republishing this material for advertising or promotional purposes, creating new collecting works, for resale or lists, or reuse of any copyrighted component of this work in other works.

(Article begins on next page)

01 November 2026

Experimental modelling uncertainty quantification for a prototype wave energy converter

Maria Luisa Celesti[a], Francesco Ferri[b] and Nicolás Faedo[a]

***Abstract*— The dynamical behaviour of wave energy conversion systems (WECs) can be described in terms of the well-known Navier-Stokes equations which, being significantly complex, preclude their use in control design and performance assessment procedures. As such, WEC devices are virtually always modelled in terms of rather simplistic dynamical representations, aiming to produce models which are tractable both from a computational, and an analytical perspective. These models, nonetheless, are inherently affected by uncertainty, introduced by the set of small motion assumptions used to derive such simplistic representations. Deriving methodologies for a sensible quantification of this uncertainty is hence fundamental to understanding the effect of these modelling assumptions in the overall control design and performance assessment procedures. This paper presents a set of experimental tests conducted on a prototype system, locked at different equilibrium positions to account for different wetted surfaces, with the objective of characterising the uncertainty introduced by assuming small device motion within WEC modelling. The corresponding modelling mismatch is quantified in the frequency-domain, and a family of WEC models is generated by means of additive uncertainty. Leveraging the identified set of systems, numerical simulations are performed to show the potential impact of this uncertainty in the performance estimation of this prototype WEC system, for different irregular sea states.**

I. Introduction

Countries worldwide are increasingly sensing the urgency to address climate change, predominantly driven by the escalating severity of extreme weather events. To combat this global challenge, there is a growing necessity to exploit renewable sources. In particular, among the avilable resources, recent efforts are addressed in exploiting the (yet largely untapped [1]) wave energy resource, which not only provides clean energy, but also seeks to protect ocean ecosystems, being a significant driver in the transition away from fossil fuels. A large number of so-called wave energy converters (WECs) concepts and prototypes can be found within the literature, which attempt at harvesting energy from ocean waves [2], [3]. A particularly well adopted technology is that featured by point absorber WEC systems, such as the device analysed within this study, which are floating structures connected to a generator for wave mechanical power transformation into available grid energy.

Modelling and control have a fundamental role to play in the pathway to WEC commercialisation [4]. In particular, efficient control of WECs, and reliable performance assessment, is crucial to reduce their cost of energy, hence enhancing their possibilities of arriving at commercialisation stage. As such, the system dynamics and control community has a major role to play, in laying the grounds and basis for optimal operation of these devices, and associated algorithms to achieve this objective, where different (and rather diverse) approaches keep being proposed [5].

The dominant dynamics of WEC systems essentially respond to the well-known set of Navier-Stokes equations, which require complex numerical routines to compute an associated solution. As such, modelling of WECs is virtually always performed adopting a set of rather limiting assumptions, with the aim of reducing the analytical and computational complexity associated with the derived structures. Particularly, small motion assumptions are widely adopted, in order to derive linear representations suitable for real-time control design procedures. Nonetheless, different from more traditional control objectives (such as tracking/regulation), WEC control systems pursue an energy-maximisation criterion, which leads to larger motion behaviour, in an effort to maximise the energy conversion from the surrounding wave field. In other words, the controller itself violates the small motion hypothesis used for modelling, leading to the so-called wave energy paradox [6]. Furthermore, standard modelling procedures pursued in the literature may even exclude essential WECs components, hence finding significantly different results in terms of expected productivity [7].

These modelling practices inevitably lead to a potentially large degree of uncertainty, which hinders the actual potential of WEC systems at the desing stage, being detrimental for the final decision making process. In fact, effectively considering modelling uncertainty affects the design of the controller and the device itself, hence influencing the overall performance [8]. As such, characterising and quantifying this uncertainty is fundamental both to obtain representative productivity results, and design control techniques able to maximise energy absorption while being aware of the corresponding uncertainty set. In fact, to achieve a robust optimal control design, taking into account a suitably quantified uncertainty set is a fundamental requirement [9], [10]. Within WECs, uncertainty quantification has been performed using CFD-based numerical tank experiments [11], with the aim of enhancing overall performance assessment. Though numerical wave tanks can be precise with extensive 'tuning', the experimental quantification of modelling uncertainty in WEC systems is fundamental to provide realistic information on the actual process, and the impact of these in the overall performance obtained with a given device. To the best of our knowledge, a

[a]M. L. Celesti and N. Faedo are with the Marine Offshore Renewable Energy Lab, Department of Mechanical and Aerospace Engineering, Politecnico di Torino, Italy (Corresponding author: M. L. Celesti marialuisa.celesti@polito.it).

[b] F. Ferri is with the Department of the Built Environment, Aalborg University, Denmark.

thorough experimental uncertainty quantification has not yet been presented in the literature, leaving a major gap towards reliable robust control and performance evaluation.

Motivated by this, this paper presents the quantification of system uncertainty based on experimental data, for a prototype WEC. A set of tailored tests, designed to quantify the modelling uncertainty introduced by the standard small motion assumptions, is executed within the wave basin facilities available at Aalborg University. The uncertainty quantification is performed in the frequency-domain while, subsequently, a corresponding family of models is generated with standard identification techniques. The experimentally identified family of models for the adopted prototype is used within an extensive numerical appraisal, in which the performance obtained for different members of this family is compared to what would be obtained if an isolated nominal model is used, *i.e.* without considering any uncertainty.

The reminder of this paper is organised as follows. Section II introduces the device characteristics and a description of the proposed tests, while Section III reports the modelling procedure used within this study. Section IV, together with Section V, represent the core of this paper, providing a formal derivation of the model uncertainty and their effect on the controlled device. Finally, Section VI encompasses the main conclusions of this paper.

II. Device and experimental test description

The WEC system used within this study is a 1:20 scaled prototype of the so-called Wavestar device [12], and is schematically depicted in Figure 1. The system consists of a floater which moves in pitch about a defined reference point, and it is adopted as a representative benchmark study. The choice of this WEC is driven by the large number of previous studies available on the prototype [13]–[16], guaranteeing the representativity of this system for experimental studies. The results presented within this study stem from an experimental campaign conducted with the aforementioned prototype device in the facilities of Aalborg University, Denmark. In particular, the WEC is tested in a basin with an active test area of 13 [m] × 8 [m] (length × width) and a fixed depth of 0.9 [m], equipped with a wavemaker system with active absorption, able to accurately emulate diverse sea state conditions. The interested reader is referred to *e.g.* [12] for a detailed discussion on this particular prototype.

The system can be seen as a single degree-of-freedom (DoF) WEC. In fact, from an hydrodynamic point of view, mutiple DoFs co-exist, although these are resolved into a single power take-off (PTO) DoF (*i.e.* rotation about point **1**). The mechanical rotation about **1** is subsequently translated into a linear motion of the arm connecting **3** and **2**, and ultimately into electrical power via the linear generator.

A. Experimental tests specification

During the experimental tests, the device is locked at different equilibrium positions, both increasing and decreasing the angle of the floater with respect to a nominal position,

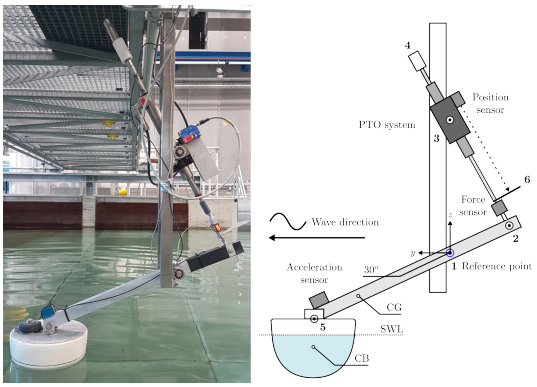
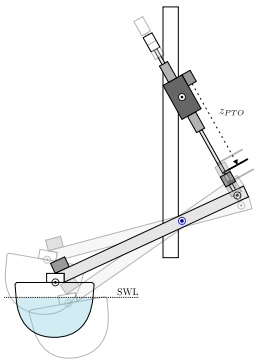


Fig. 1: Photo (left) and schematic illustration (right) of the Wavestar device.



(a) Schematic illustration of the variation in position.

Position	z_{PTO} [mm]	θ [°]
1	20	24.30
2	10	27.15
0	0	30
3	-10	32.85
4	-20	35.70

(b) Position specification for uncertainty quantification tests.

Fig. 2: Uncertainty quantification test specifications.

placed in line with the still water level (SWL). This is performed to characterise the behaviour of the system for diverse equilibrium positions, in order to quantify the uncertainty introduced by the standard small motion assumptions about a nominal SWL (see the discussion provided in Section I). In the nominal position, indicated in Figure 2b with 0, the floater arm stands at approximately 30° with respect to the SWL (see Figure 1). The locking position is linearly changed with a fixed step of 10 [mm] along the z_{PTO} direction, reported with a dashed arrow in Figure 2a, adopting the nominal position as the baseline reference (0 [mm]).

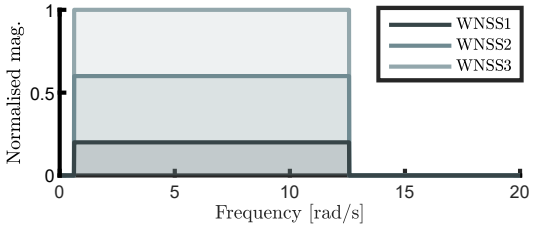


Fig. 3: White noise waves theoretical spectra.

Within the experimental campaign, and to provide an empirical characterisation of the device dynamics in each locking position, white noise waves are employed as identification sea states, according to the spectra described within Figure 3. In fact, white noise spectra, with a constant spectral

density function in a sufficiently large frequency range, can provide an accurate characterisation of the input/output behaviour associated with the WEC, which potentially operates in a wide range of sea conditions. Different white noise waves are generated within the basin, with a constant frequency range (covering the main WEC dynamics) and an increasing energy content, that translates into a larger free-surface elevation. The same waves are emulated for each different locking position (as per Figure 2b).

Subsequently, a measure of the so-called wave excitation force/torque acting on the WEC, for each specific free-surface elevation generated within the wave tank, and every single locking position tested, is obtained. To perform the measurements, the device is blocked by locking the PTO motor shaft, and the force exerted by each wave is measured directly via the load cell attached to point **2**. Finally, the device displacement and velocity are measured in free-motion conditions, *i.e.* unlocked, producing a corresponding set of motion outputs for each tested white noise sea state.

Note that part of the experimental data used within this study is included in the dataset reported in [17], where a wider description of the experimental setup is offered. Nonetheless, tests on different locking positions are performed specifically for this study, with the aim to highlight the influence of different wetted surfaces on the wave-to-excitation force dynamics. In particular, as discussed within Section I, relatively large motions can invalidate the standard linearity assumptions, in which WECs normally operate under controlled conditions. This can be represented in terms of a set of different input/output (force-to-velocity, in this case) mappings associated to the WEC system, rather than a unique one, as further specified in Section III.

III. Force-to-velocity model determination

The first objective is to characterise, for each different locking position considered, the force-to-velocity mapping. As per described in Section II-A, the generation of wave elevation is performed considering white noise waves as inputs, while the corresponding force, f_e, is obtained through load cell measurements (see Section II).

Achieving the characterisation of the force-to-velocity mapping, $f_e \mapsto v$, means to characterise the operator $G : \mathbb{C} \to \mathbb{C}$, considering the force f_e as input, and the velocity v as output of the system. In this study, the empirical mapping computation is addressed via a frequency domain black-box-identification methodology (see [18]). In particular, applied inputs can be described by the set $\mathscr{F} = \{f_{e_i}^j\}_{(i,j)\in\mathcal{I}_i\times\mathcal{I}_j}$, where $\mathcal{I}_i = \{0,1,2,3,4\}$, contains the different locking positions, while the set $\mathcal{I}_j = \{1,2\}$ refers to the input sea-states considered. The force inputs, $\mathscr{F}$, produce an associated set of velocity outputs $\mathscr{V} = \{v^j\}_{j\in\mathcal{I}_j}$.

Using capital letters to indicate Fourier transform pairs, *e.g.* $F_i^j(\jmath\omega)$ for $f_{e_i}^j(t)$, a non-parametric frequency-domain characterisation can be computed in terms of the so-called empirical transfer function estimate (ETFE):

$$\tilde{G}_i^j(\jmath\omega) = \frac{V^j(\jmath\omega)}{F_i^j(\jmath\omega)}. \tag{1}$$

An average of input/output pairs, associated with different incoming sea-states, is performed to produce a low variance set, computed as:

$$\bar{G}_i(\jmath\omega) = \frac{1}{\#\mathcal{I}_j}\sum_{j=1}^{\#\mathcal{I}_j}\tilde{G}_i^j(\jmath\omega). \tag{2}$$

To further improve the quality of the identification, by splitting the dataset, *i.e.* system input and output signals, a Bartlett-type average [19] is performed, while a moving average filter is applied to (1). Finally, a parametric approximation of the corresponding response operator, G_i, is computed considering standard system identification techniques. Within this study, subspace-based techniques based on [20] are employed, providing an associated finite-dimensional continuous-time state-space system.

In particular, Figure 4 shows the Bode plot associated with the device in the nominal position, featuring the synthesis of the identification procedure. In fact, each single ETFE is reported within Figure 4, computed in terms of each performed experiment (blue lines with transparency), together with their average, $\bar{G}_0$, computed as in (2) (light blue line), its filtered version, $\bar{G}_{f_0}$ (green line), and the response characterising the identified state-space model, G_0 (black line).

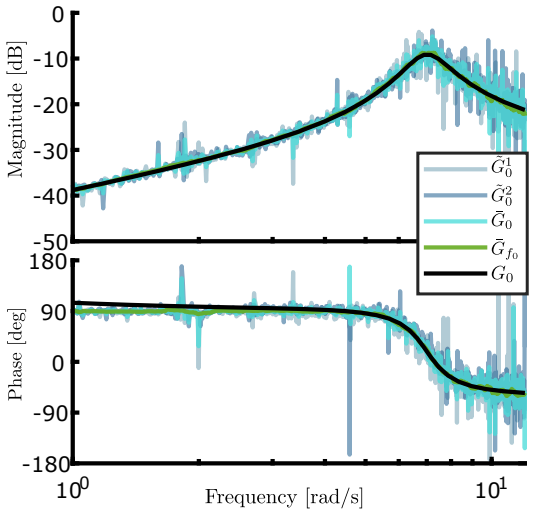


Fig. 4: Identification procedure for the nominal position.

The procedure is repeated for each different locking position, to obtain a corresponding parametric form. Figure 5 presents a comparison, in terms of magnitude and phase, of the identified parametric mappings, for each different locking position. Furthermore, in the same figure, the systems identified using experimental data are compared with the numerical characterisation of the device based on potential flow theory, computed employing the boundary element method (BEM) solver, NEMOH [21]. Note that the latter, which even shows a different resonance behaviour, is effectively the standard modelling procedure employed within the literature to derive a dynamical WEC model for control and performance assessment purposes.

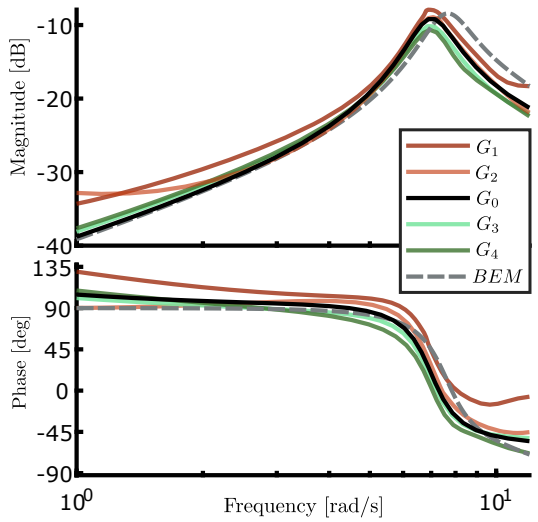


Fig. 5: Comparsion of the identified force-to-velocity model depending on the different positions, and BEM response (dashed).

IV. Uncertainty Characterisation

ETFEs obtained from the experimental data are now considered to quantify the model uncertainty. The uncertainty region, at a specific frequency point, is calculated based on the maximum distance between the parametric model and the ETFEs associated with each different sea-state at that frequency. In particular, for a given $i \in \mathcal{I}_i$, this value can be defined such that,

$$|W_{\Delta,i}(\jmath\omega)| = \max_{j \in \mathcal{I}_j} \left| \tilde{G}_i^j(\jmath\omega) - G_i(\jmath\omega) \right|, \qquad (3)$$

where $\tilde{G}_i^j(\jmath\omega)$ is the ETFE, associated to each specific sea-state, computed as in (1), while $G_i(\jmath\omega)$ is the frequency-response corresponding to each parametric model. The same information given by the magnitude of $W_{\Delta,i}(\jmath\omega)$, is shown in Figure 6 on a polar (Nyquist) plot, for each different locking position. Depending on the specific considered position, a different uncertainty bound is obtained, as clearly visible in the complex plane plots.

Considering the so-called nominal position, which effectively corresponds with the SWL line considered within the literature, a further definition is given:

$$|W_{\Delta,n}(\jmath\omega)| = \max_{(i,j) \in \mathcal{I}_i \times \mathcal{I}_j} \left| \tilde{G}_i^j(\jmath\omega) - G_0(\jmath\omega) \right|, \qquad (4)$$

where $G_0(\jmath\omega)$ is the frequency response of parametric model associated with the nominal position. This definition, by comparing the nominal case with the set of ETFEs associated with each locking position and sea state considered, provides an estimation of the worst case scenario that can be encountered, in terms of uncertainty, for the considered WEC system.

Figure 7 presents, for the nominal case, a superposition of the uncertainty as defined in equation (3) (grey lines), and $W_{\Delta,n}(\jmath\omega)$ (red lines). It is readily apparent that the latter disk radius exhibits a considerable increase in size with respect to that computed according to equation (3), hence depicting the worst case scenario encounterable due to the standard small motion assumptions considered within the literature.

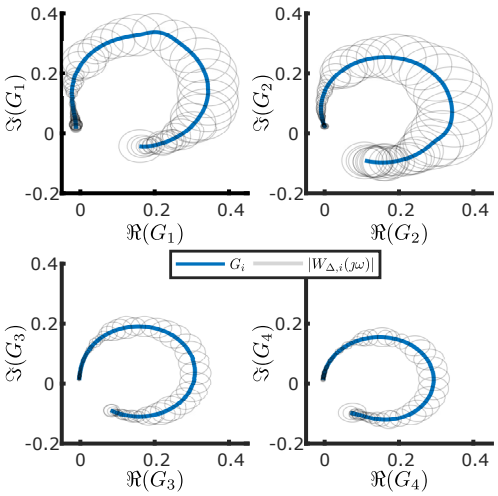


Fig. 6: Uncertainties with respect to the each locking positions.

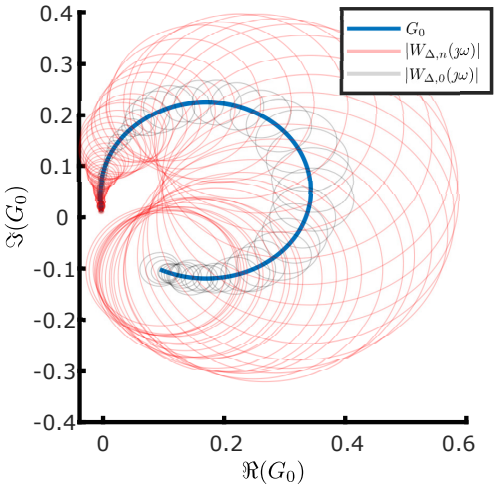


Fig. 7: Uncertainties with respect to the nominal position worst case scenario (red).

The latter uncertainty bound is used, in the following, to generate a family of systems, *i.e.* a group of plants that are included into the range defined by the uncertainties, as further specified in Section V.

V. Performance in Controlled Conditions

Generally, as discussed within Section I, the control objective for WECs is to maximise converted energy. This translates to adapting the WEC characteristics (*e.g.* resonance) to the operating conditions, *i.e.* to different waves and wave climates [4]. Though fundamental to achieve a reliable WEC operation, robustness issues, in this field, are not yet widely addressed, and this is mainly due to the non-traditional control objective. As such, robust control techniques are essential in ensuring optimal performance of WEC systems under varying environmental conditions. Addressing and characterising the underlying uncertainties,

with a subsequent integration of robust control, is crucial to improving the reliability and performance of WECs.

Within this study, leveraging the uncertainty bounds defined in equation (4) through experimental data, a family of models is generated starting from the so-called nominal position. Hence, the nominal model, characterised experimentally, is considered, along with a suitably defined dynamical deviation. The deviations, characterised in terms of additive uncertainty, are used to generate a family of models for the Wavestar device, covering the uncertainty generated by assuming a constant wetted surface. Within such a framework, the response of the actual plant can be defined in terms of the set:

$$\mathcal{G} : \{G \in \mathcal{RH}_\infty \mid G = G_0 + W_{\Delta,n}\Delta\}, \tag{5}$$

where Δ is an arbitrary proper and stable transfer function satisfying the norm condition:

$$\|\Delta\|_\infty = \sup_\omega |\Delta(\jmath\omega)| \leq 1. \tag{6}$$

Figure 8 illustrates the considered family of models (20 representative plants), in the frequency-domain, with the nominal plant represented with a solid blue line.

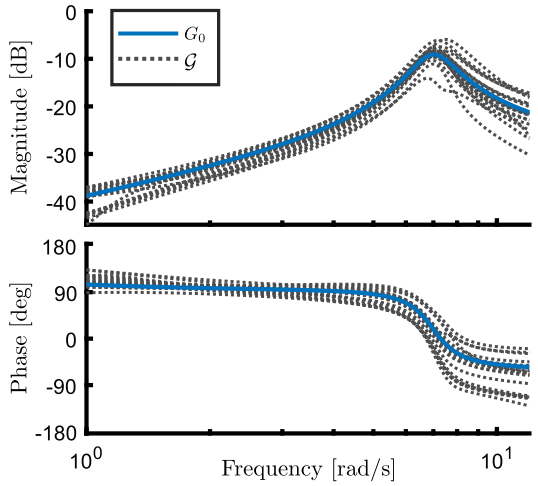


Fig. 8: Defined family $\mathcal{G}$. The nominal model is indicated with a blue line.

A. Control structure

The WEC control objective is that of maximising the absorbed energy from ocean waves over a finite time interval, T, and can be defined by the following expression:

$$J(u) = \int_T v(t)u(t)dt, \tag{7}$$

where u denotes the control (PTO) force, while v represents the device velocity. The control input is designed following the standard procedure adopted within the WEC literature, *i.e.* based on the nominal model, G_0, using the well-established "reactive" controller, which features a proportional-integral structure:

$$u(t) = Pv(t) + I\int v(t)\mathrm{d}t. \tag{8}$$

The control parameters, P and I, are computed with an optimisation procedure. In particular, within such a synthesis, the maximisation of energy is considered alongside the stability of the closed-loop, *i.e.*

$$\begin{aligned} \max_{\{P,I\}\subset\mathbb{R}} \; & J(u) \quad \text{subject to:} \\ & \text{WEC nominal dynamics } G_0, \\ & \mathcal{Z} : \{s \in \mathbb{C} \mid 1 + G_0K = 0\} \subset \mathbb{C}_{<0}, \end{aligned} \tag{9}$$

indicating with K the transfer function associated with (8). The stability condition is satisfied by ensuring that the zeros associated with the characteristic equation of the closed-loop belongs to $\mathbb{C}_{<0}$.

The control parameters are obtained for the nominal model, for each considered sea-state. In particular, within this study, for controller evaluation purposes, a set of irregular waves are generated within the wave basin with characterising parameters reported in Table I. Note that the hydrodynamic resonance for this device is located at approximately 7 [rad/s], meaning that the considered sea-states effectively represent realistic operating conditions for this prototype system.

TABLE I: Characterisation of the considered sea states for evaluation purposes based on the JONSWAP spectral formulation with significant height, H_s, peak period, T_p, and peak-enhancement factor, γ.

Sea-state	H_s [m]	T_p [s]	γ
SS1	0.063	1.412	3.3
SS2	0.104	1.836	3.3
SS3	0.0208	0.988	1

Table II reports the proportional and integral parameters associated with each sea state used for performance evaluation. The controller, based on the nominal system, is then considered within simulation, with the same parameters, for each member of the family defined in equation (5).

TABLE II: Control parameters for different sea-states.

Parameters	SS1	SS2	SS3
P	7.498	12.856	4.736
I	-11.739	-12.383	-0.041

A numerical appraisal of the absorbed power is offered in Figure 9. In particular, this figure presents the difference between the power obtained for G_0, (*i.e.* in idealised conditions - without considering any uncertainty within evaluation) and that generated with each component of the uncertain family, normalised with the respect to the former. The procedure is then repeated for each of the irregular sea-states. The results are presented in terms of the normalised error defined as:

$$E = \frac{P_{G_0} - P_G}{P_{G_0}}, \tag{10}$$

where P_{G_0} is the absorbed power of the nominal model, while P_G is the power associated with the 20 representatives models chosen from the corresponding family (see Figure 8),

i.e. $G \in \mathcal{G}$, and it can take values up to 50%, indicating a significant variation in performance assessment when effectively considering the uncertainty set.

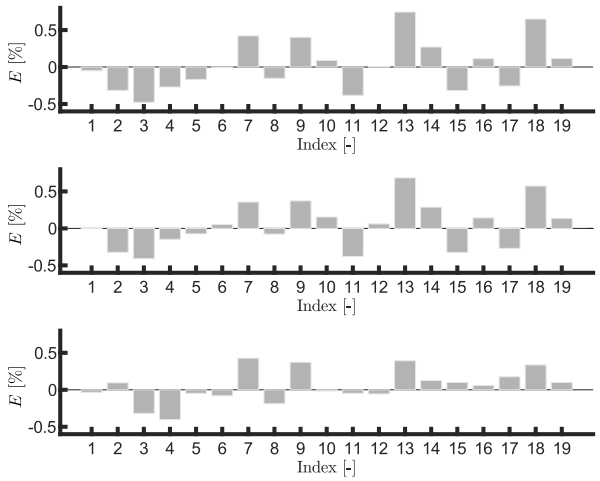


Fig. 9: Power obtained with the system in the set $\mathcal{G}$ for sea-states ISS1,ISS2,ISS3. The index indicates an element considered from the family (5), generated randomly.

Changing the assessment input, *i.e.* the operating conditions, can also lead to a variation in the absorbed power between the nominal device, G_0, and any potential element belonging to the set $\mathcal{G}$. However, the most noticeable effect is linked to the considered member of the family, defined depending on the worst-case scenario due to the different SWL position. Hence, designing the controller only based on information of the so-called nominal model, immediately translates into a variation of the system productivity. This leads to a mismatch between expected and actual device productivity, leading to an innacurate characterisation of performance, which can be detrimental at the design stage.

VI. Conclusions

This paper proposes an experimental characterisation of the modelling uncertainty introduced by small motion assumptions in linear WEC structures, for a well-known prototype system. In particular, different device equilibrium positions are considered, generating diverse responses according to the corresponding wetted surface. The obtained responses are leveraged to compute an empirical characterisation of the uncertainty in the frequency-domain, hence providing a suitable family of models for the particular prototype. The obtained set of systems is then used to evaluate performance for a controller designed solely based on a nominal equilibrium position, showing that the productivity, computed taking into account the uncertainty set, can exhibit large variations, leading to a potentially large mismatch. Future work will exploit the proposed experimental uncertainty quantification procedure for robust optimal control design purposes, leveraging techniques such as those outlined in [9], [10].

References

[1] G. Mork, S. Barstow, A. Kabuth, and M. T. Pontes, "Assessing the global wave energy potential," in *International Conference on Offshore Mechanics and Arctic Engineering*, vol. 49118, 2010, pp. 447–454.

[2] A. F. O. Falcão, "Wave energy utilization: A review of the technologies," *Renewable and Sustainable Energy Reviews*, vol. 14, pp. 899–918, 2010.

[3] J. Falnes and A. Kurniawan, *Ocean waves and oscillating systems: linear interactions including wave-energy extraction*. Cambridge university press, 2020, vol. 8.

[4] J. V. Ringwood, S. Zhan, and N. Faedo, "Empowering wave energy with control technology: Possibilities and pitfalls," *Annual Reviews in Control*, 2023.

[5] E. Pasta, N. Faedo, G. Mattiazzo, and J. V. Ringwood, "Towards data-driven and data-based control of wave energy systems: Classification, overview, and critical assessment," *Renewable and Sustainable Energy Reviews*, vol. 188, p. 113877, 2023.

[6] C. Windt, N. Faedo, M. Penalba, F. Dias, and J. V. Ringwood, "Reactive control of wave energy devices–the modelling paradox," *Applied Ocean Research*, vol. 109, p. 102574, 2021.

[7] B. Paduano, F. Carapellese, E. Pasta, N. Faedo, and G. Mattiazzo, "Optimal controller tuning for a nonlinear moored wave energy converter via non-parametric frequency-domain techniques," *Trends in renewable energies offshore*, pp. 393–400, 2022.

[8] F. Giorcelli, S. A. Sirigu, D. Basile *et al.*, "Relevance of robustness and uncertainties analysis in the optimal design of wave energy converters," in *Proceedings of the European Wave and Tidal Energy Conference*, vol. 15, 2023.

[9] D. Garcia-Violini and J. V. Ringwood, "Energy maximising robust control for spectral and pseudospectral methods with application to wave energy systems," *International Journal of Control*, vol. 94, no. 4, pp. 1102–1113, 2021.

[10] N. Faedo, G. Mattiazzo, and J. V. Ringwood, "Robust energy-maximising control of wave energy systems under input uncertainty," in *2022 European Control Conference (ECC)*. IEEE, 2022, pp. 614–619.

[11] M. Farajvand, V. Grazioso, D. García-Violini, and J. V. Ringwood, "Uncertainty estimation in wave energy systems with applications in robust energy maximising control," *Renewable Energy*, vol. 203, pp. 194–204, 2023.

[12] R. H. Hansen and M. M. Kramer, "Modelling and control of the Wavestar prototype," in *Proceedings of the 9th European Wave and Tidal Energy Conference, EWTEC 2011*. University of Southampton, 2011.

[13] J. Ringwood, F. Ferri, N. Tom, K. Ruehl, N. Faedo, G. Bacelli, Y.-H. Yu, and R. G. Coe, "The wave energy converter control competition: Overview," in *International conference on offshore mechanics and arctic engineering*, vol. 58899. American Society of Mechanical Engineers, 2019, p. V010T09A035.

[14] C. Windt, N. Faedo, D. García-Violini, Y. Peña-Sanchez, J. Davidson, F. Ferri, and J. V. Ringwood, "Validation of a CFD-based numerical wave tank model of the 1/20th scale Wavestar wave energy converter," *Fluids*, vol. 5, no. 3, p. 112, 2020.

[15] S. Heo and W. Koo, "Dynamic response analysis of a wavestar-type wave energy converter using augmented formulation in Korean nearshore areas," *Processes*, vol. 9, no. 10, p. 1721, 2021.

[16] N. Tom, K. Ruehl, and F. Ferri, "Numerical model development and validation for the WECCCOMP control competition," in *International Conference on Offshore Mechanics and Arctic Engineering*, vol. 51319. American Society of Mechanical Engineers, 2018, p. V010T09A042.

[17] N. Faedo, Y. Peña-Sanchez, E. Pasta, G. Papini, F. D. Mosquera, and F. Ferri, "SWELL: An open-access experimental dataset for arrays of wave energy conversion systems," *Renewable Energy*, vol. 212, pp. 699–716, 2023.

[18] L. Ljung, "System identification," in *Signal analysis and prediction*. Springer, 1998, pp. 163–173.

[19] M. S. Bartlett, "Smoothing periodograms from time-series with continuous spectra," *Nature*, vol. 161, no. 4096, pp. 686–687, 1948.

[20] T. McKelvey, H. Akçay, and L. Ljung, "Subspace-based multivariable system identification from frequency response data," *IEEE Transactions on Automatic control*, vol. 41, no. 7, pp. 960–979, 1996.

[21] A. Babarit and G. Delhommeau, "Theoretical and numerical aspects of the open source BEM solver NEMOH," in *11th European wave and tidal energy conference (EWTEC2015)*, 2015.